SPECTRAL DECOMPOSITION WITH SPARSITY CONSTRAINT AND ITS APPLICATION

HAN XU[1], XINWEN WANG[1] and LI GAO[2]

[1] *School of Earth Sciences and Recourses, China University of Geosciences, Beijing 100083, P.R. China. xuhan_cug2016@126.com, wxw@cugb.edu.cn*
[2] *Institute of Geomechanics, Chinese Academy of Geological Sciences, Beijing 100081, P.R. China. gl1989@126.com*

(Received December 2, 2016; revised version accepted November 10, 2017)

ABSTRACT

Xu, H., Wang, X. And Gao, L., 2018. Spectral decomposition with sparsity constraint and its application. *Journal of Seismic Exploration*, 27: 89-101.

Spectral decomposition has been widely used in seismic signal processing and interpretation at present because it can reveals lots of valuable information hidden in the broadband seismic response. Unlike the conventional frequency-based methods, spectral decomposition is able to estimate the frequency contents of the signal at the specific time. How to seek an optimal solution is the most significant aspect for Spectral Decomposition with Sparsity Constraints (SDSC). In this paper, the L_1 regularized L_2-norm is employed as the objective function, the Ricker wavelet is chosen to construct a wavelet library and the optimal solution is obtained by the Iterative Soft Thresholding Algorithm (ISTA). We apply SDSC to the synthetic and field examples. The former show that the SDSC method does a better job in both time and frequency resolution than the traditional spectral decomposition technique, namely the continuous wavelet transform (CWT) method, which always suffers from the conflict between time resolution and frequency resolution. Applications to field data further indicate the potential of the SDSC method in identifying the strong anomalies related to hydrocarbon, and detecting the variations in amplitude associated with faulting.

KEY WORDS: spectral decomposition sparsity constraint; continuous wavelet transform, hydrocarbon detection, fault identification.

INTRODUCTION

Spectral decomposition has proven a powerful tool in reservoir characterization (Chen et al., 2014; Radad et al., 2016), and has been utilized for thin bed analysis (Partyka et al., 1999), subsurface structures and reefs for identification (Marfurt and Kirlin, 2001; Liu and Marfurt, 2007),

0963-0651/18/$5.00

seismic attenuation estimation (Reine et al., 2009), ground-roll suppression (Liu and Fomel, 2013; Liu et al., 2016), random noise attenuation (Bonar, 2013), hydrocarbon indicator (Castagna et al., 2003; Farfour et al., 2013; Chen et al., 2014), and seismic dispersion anomalies and channel sands detection (Odebeatu et al., 2006; Wu et al., 2014). Currently, many approaches have been developed for spectral decomposition. The short time Fourier transform (STFT) is commonly used, which generates a localized time-frequency representation of a time series by applying Fourier transform on windowed seismogram (Allen, 1977). However, the window length has a strong impact on time-frequency resolution, specifically, a small window is well resolved in time but poorly resolved in frequency, whereas, a larger window is poorly resolved in time but well resolved in frequency. Subsequently, this drawback of STFT is overcome by continuous wavelet transform (CWT), where wavelets dilate in such a way that the time support changes for different frequencies. Smaller time support increases the frequency support, which shifts toward higher frequencies. Similarly, larger time support decreases the frequency support, which shifts toward lower frequencies. Thus, when the time resolution increases, the frequency resolution decreases, and vice versa (Rioul et al., 1991; Sinh et al., 2005). The S transform is a combination of STFT and WT, it not only eliminates extra requirement of setting a window length for STFT but also is characterized by multi-resolution analysis of WT (Stockwell et al., 1996). Wigner-Ville distribution (Jeffrey, 1999) and Cohen distribution (Cohen, 1966) have higher time-frequency resolution, but the existence of interference or cross-product terms limits their application. Matching pursuit (Mallat, 1993) obtains time-frequency representation by decomposing the signal in time-frequency atom library which has been created. Despite its higher time-frequency resolution, this occurs at the expense of heavy computational cost due to the redundancy of atom library. Portniaguine and Castagna (2004) described seismic signal spectral decomposition as an inverse problem.

The conventional spectral decomposition aims at decomposing the seismic signal using some basis functions and the projection of it is referred as time-frequency map. Although the physical meaning of this approach is very clear and the algorithm is relatively simple, its time-frequency resolution severely depends on the chosen basis functions. Furthermore, a priori information is also not easily added to spectral decomposition procedure. In this paper, the sparsity constraint is introduced into spectral decomposition, which is described as an inverse problem solved by an Iterative Soft Thresholding Algorithm (ISTA). (Daubechies et al., 2004) We apply Spectral Decomposition with Sparsity Constraint (SDSC) to the synthetic and field examples to illustrate its potential in identifying the strong anomalies related to hydrocarbons and detecting the variations in amplitude associated with faulting.

THEORY

The convolution model states that a seismic trace, $s(t)$, is composed of the convolution of a wavelet, $w(t)$, and the reflectivity sequence, $r(t)$, with random noise $n(t)$ (Robinson and Treitel, 1980).

$$s(t) = w(t) * r(t) + n(t) \quad . \tag{1}$$

However, eq. (1) cannot reflect the relationship between frequency and time. Therefore, as illustrated in Bonar et al. (2010), a seismic trace can be described as the convolution of multiple wavelets composed of different frequency contents and pseudo-frequency dependent reflectivity with additive noise.

$$s(t) = \sum_{m=1}^{M} \left[w_m(t) * r_m(t) \right] + n(t) \tag{2}$$

where $w_m(t)$ denotes the specific wavelet and its dominant frequency is related with m. $r_m(t)$ is the wavelet-dependent reflectivity series. The advantage of using eq. (2) to represent the seismic trace is that the wavelet-dependent reflectivity series is capable of highlighting that frequency content corresponding to $w_m(t)$ in the signal $s(t)$.

In terms of linear algebra, eq. (2) can also be written as:

$$s = \begin{pmatrix} W_1 & W_2 & \mathrm{L} & W_M \end{pmatrix} \begin{pmatrix} \mathrm{R}_1 \\ R_2 \\ \mathrm{M} \\ R_M \end{pmatrix} + n = Dx + n \quad , \tag{3}$$

where s is the seismic signal, x is an ensemble of wavelet-dependent reflectivity series $\{R_m, m = 0\ 1,2,\mathrm{K},\mathrm{M}\}$, D is the convolution matrix library, W_m and R_m are the frequency-dependent wavelet convolution matrix and reflectivity series, respectively, which can be represented as:

$$W_m = \begin{bmatrix} w_N, w_{N-1}, \mathrm{L}\ , w_1, 0, 0, \mathrm{L}\ , 0 \\ 0, w_N, w_{N-1}, \mathrm{L}\ , w_1, 0, \mathrm{L}\ , 0 \\ \mathrm{M} \\ 0, 0, 0, \mathrm{L}\ , w_N, w_{N-1}, \mathrm{L}\ , w_1 \end{bmatrix} \qquad R_m = \begin{bmatrix} r_1 \\ r_2 \\ \mathrm{M} \\ r_L \end{bmatrix} \quad , \tag{4}$$

where the size of W_m and R_m are $(N + L - 1) \times L$ and $L \times 1$, respectively.

If the noise is not considered, the local time-frequency representation can be obtained by solving eq. (5).

$$x = D^{-1} s \quad . \tag{5}$$

However, if D is not be invertible, eq. (5) cannot be solved. To combat this issue, eq. (3) can be multiplied by the conjugate transpose of D. In general, $D^H D$ is invertible. Thus, the solution of eq. (3) can be expressed as:

$$x = (D^H D)^{-1} D^H s \quad . \tag{6}$$

To obtain x mentioned above is equivalent to minimizing the following objective function J.

$$J = \|s - Dx\|_2^2 \quad , \tag{7}$$

where $\|g\|_2^2$ denotes the L_2 norm.

Eq. (7) may be unstable in the presence of noise. Therefore, it is necessary to add an additional constraint on x. The resulting objective function is given by (Donoho, 2006).

$$J = \frac{1}{2}\|s - Dx\|_2^2 + \lambda \|x\|_1 \quad , \tag{8}$$

where $\|g\|_1$ denotes the L_1 norm, λ is the sparsity factor.

There are many algorithms for solving eq. (8), in this paper, we use ISTA to solve it, which is a proximal gradient descent method, also known as Landweber iteration method (Landweber, 1951). The i-order recursion formula is written as:

$$x_{i+1} = x_i + \frac{1}{\alpha} D^H \left(s - Dx_i\right) \quad , \tag{9}$$

where α is used to control the convergence rate.

The gradient descent method can also be equivalently posed through the proximal regularization of the cost function at x_{i-1} according to (Beck and Teboulle, 2009).

$$x_i = \min \left\{ J\left(x_{i-1}\right) + \left\langle x - x_{i-1}, \nabla J\left(x_{i-1}\right)\right\rangle + \frac{\alpha}{2}\|x - x_{i-1}\|_2^2 \right\} \quad , \tag{10}$$

where $\langle x, y \rangle = x^T y$.

If the constant terms are ignored, eq. (10) can be rewritten as:

$$x_i = \min \left\{ \frac{\alpha}{2} \left\| x - \left[x_{i-1} - \frac{1}{\alpha} \nabla J\left(x_{i-1}\right) \right] \right\|_2^2 \right\} \quad . \tag{11}$$

Because the L_1 norm for the cost function in eq. (8) is separable, its minimization is not affected by the minimization of the data misfit term. Therefore, the minimization of a slightly easier optimization problem,

$$J = \|s - x\|_2^2 + \lambda \|x\|_1 \tag{12}$$

is used to serve as an analogy for minimizing eq. (8) (Selesnick, 2009). Here, it is assumed that s and x have the same dimensions. If we set the derivative of eq. (12) with respect to x is equal to zero, eq. (13) can be obtained.

$$s = x + \frac{\lambda}{2}\mathrm{sgn}(x) \quad . \tag{13}$$

The solution of eq. (13) is defined by:

$$x = T_{\lambda/2}(s) \quad , \tag{14}$$

where $T_\lambda(g)$ denotes the soft thresholding. For a complex number $Ae^{i\theta}$, the soft thresholding is defined as:

$$T_\lambda\left(Ae^{i\theta}\right) = \begin{cases} (A-\lambda)e^{i\theta} & A > \lambda \\ 0 & A < \lambda \end{cases} \quad . \tag{15}$$

Through this analogy, the minimization of eq. (8) can be written as follows:

$$x = T_{\lambda/2}\left(\nabla\left(\|s - Dx\|_2^2\right)\right) \quad . \tag{16}$$

The iterative solution for the minimization of eq. (8) provided by ISTA becomes,

$$x_{i+1} = T_{\lambda/2\alpha}\left(x_i + \frac{1}{\alpha}D^H\left(s - Dx_i\right)\right) \quad , \tag{17}$$

where α is a constant greater than the maximum eigenvalue of DD^H.

EXAMPLES

Synthetic example

In this section, we first take a simple synthetic time series as an example in order to demonstrate the SDSC's high resolution both in time and frequency. The synthetic trace [Fig.1 (a)] is composed of a 50 Hz central frequency Ricker wavelet located around 0.1 s, a 90° phase rotated 40 Hz central frequency Ricker wavelet located around 0.25 s, a 20 Hz central

frequency Ricker wavelet of negative amplitude located around 0.4 s, and two close Ricker wavelet with 30 Hz central frequency located around 0.6 s. As a reference, the CWT is also applied to the same data. Figs. 1(b) and 1(c) show the spectral decomposition results using CWT and SDSC, respectively. As can be seen, there is very clear difference between them, the SDSC exactly capture the five components that compose the synthetic signal and obtain a higher time-frequency resolution, which makes it more obvious that there are two completely separated events around 0.6 s. In contrast, the CWT shows a poor performance owing to the low resolution both in time and frequency. To access the impact of noise on spectral decomposition, a noisy synthetic trace is tested and the results based on CWT and SDSC are displayed in Figs. 2(b) and 2(c), respectively. It can be seen that the time-frequency map of CWT become relatively poor because of the presence of noise, however, the result of SDSC is less sensitive to noise and it can still reflect that main components comprised the noisy signal well. In this sense, the SDSC method does a better job.

In addition, in order to further illustrate the applicability of the SDSC approach, a real seismic trace is considered, which is depicted in Fig. 3(a). The spectral decomposition results using CWT and SDSC are shown in Figs. 3(b) and 3(c), respectively. It can be easily observed that the SDSC presents a sparser time-frequency representation compared with CWT, and it is still able to track the time-frequency energy locating the main seismic events in the trace effectively.

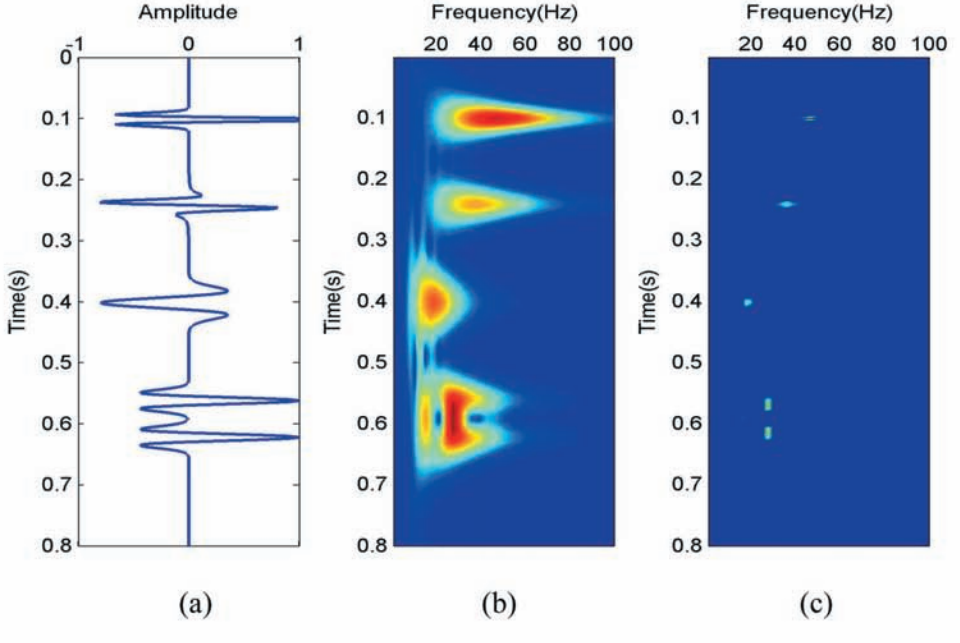

Fig. 1. (a) Synthetic signal composed of Ricker wavelets with different frequency and phase. (b) Time-frequency map obtained by using CWT. (c) Time-frequency map obtained by using SDSC. The SDSC method shows a sparse spectral decomposition result.

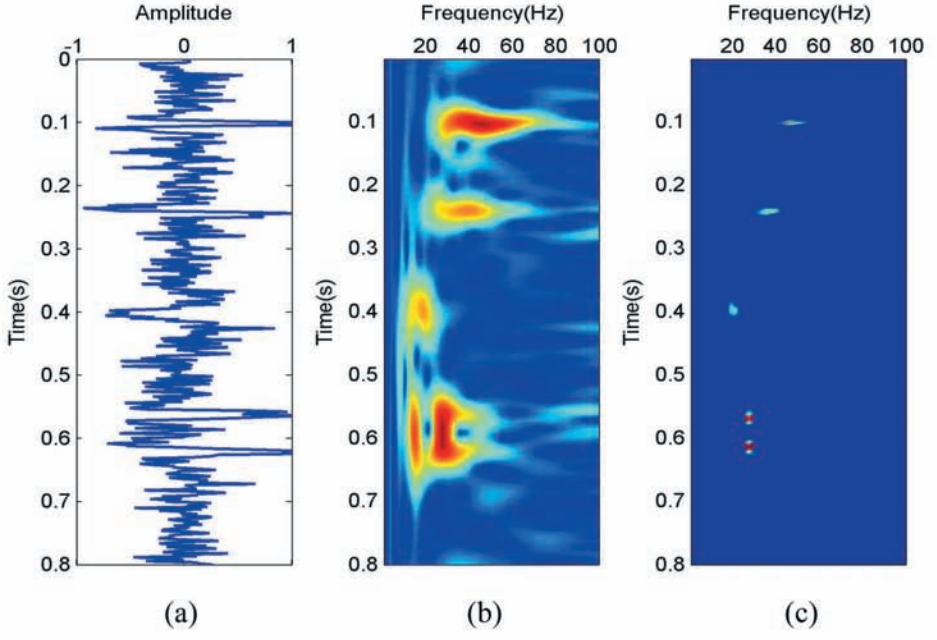

Fig. 2. (a) Noisy synthetic signal. (b) Time-frequency map obtained by using CWT. (c) Time-frequency map obtained by using SDSC. The SDSC method can still reveal that main components comprised the noisy signal well.

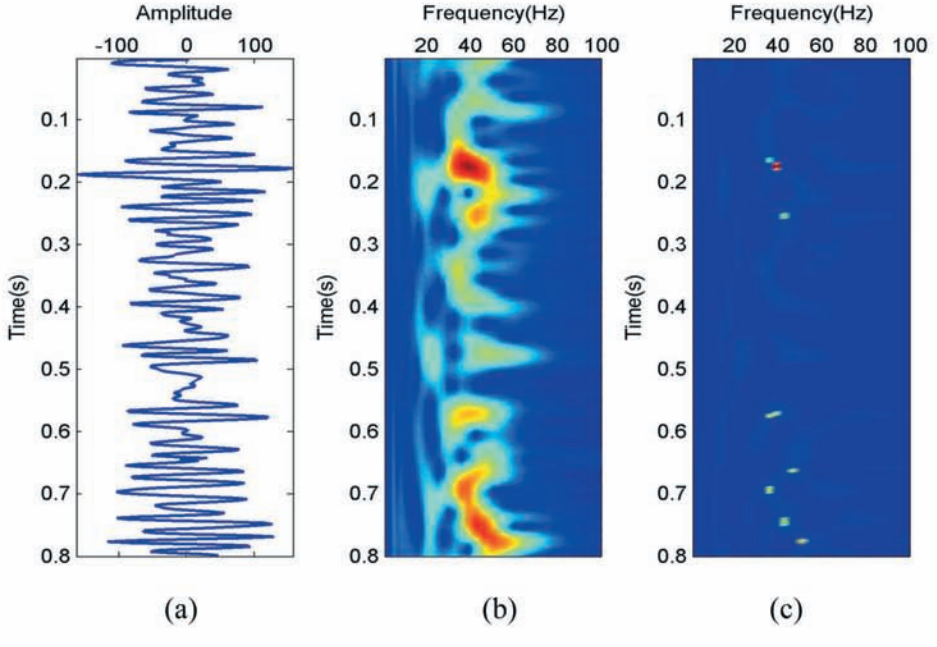

Fig. 3. (a) A real seismic trace. (b) Time-frequency map obtained by using CWT. (c) Time-frequency map obtained by using SDSC. The SDSC method is still able to capture the main seismic events effectively.

Field examples

It is well known that hydrocarbon can cause the high-frequency components of a seismic signal to decaying rapidly as a seismic wave passes through it, which results in the low-frequency shadow on seismic section. The low-frequency anomalies associated with gas-charged reservoir have been utilized as a substantiating hydrocarbon indicator (Castagna et al., 2003). In this section, we first utilize the gas-filled sand reservoir (Fig. 4) as an example to validate the SDSC for the detection of hydrocarbon. This data consists of 60 traces, the time range is from 3.5 s to 4.5 s with the time sampling interval of 2 ms. The zone of interest indicated by the arrow is around 4 s, which has been proved to hold gas.

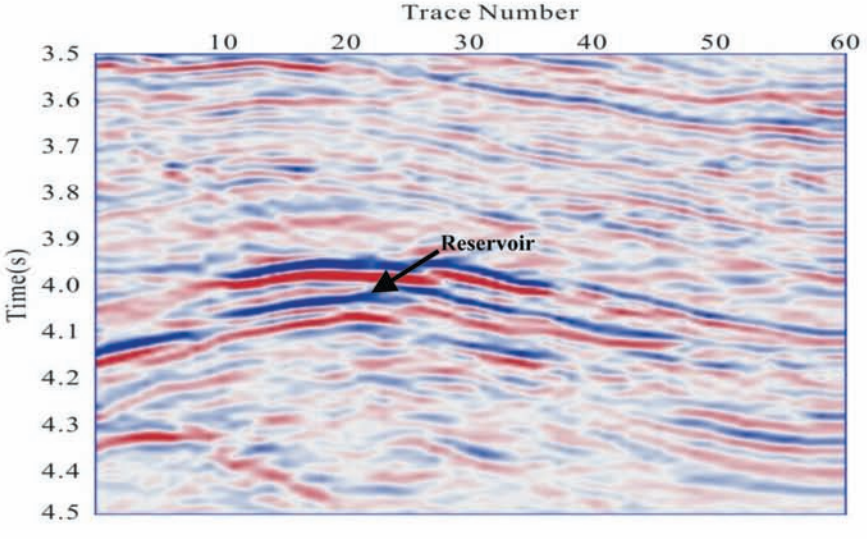

Fig. 4. The real seismic section. The arrow indicates a gas-charged reservoir.

Figs. 5(a), 5(c) and 5(e) show the common frequency slices of 20 Hz, 30 Hz and 40 Hz, respectively, obtained by using CWT method. The results from the SDSC-based method are displayed in Figs. 5(b), 5(d) and 5(f), which correspond to 20 Hz, 30 Hz and 40 Hz, respectively. As we seen from Fig. 5, the two methods exhibit the similar property, that is to say, the low-frequency anomaly is very obvious near the gas-bearing reservoir at 20Hz, and then the amplitude is gradually attenuated at 30 Hz, until it is nearly disappeared at 40 Hz. Unlike CWT, the SDSC method provides higher time-frequency resolution than CWT-based approach, which is beneficial to delineate the location and extent of the gas-filled sand reservoir more precisely. Besides, the energy between frequency slices from SDSC-based results is attenuated more rapidly as frequencies increase and the variations in amplitude are more clear, which means that the SDSC method is more sensitive to gas-charged sand and is more helpful to detect the low frequency anomaly related with hydrocarbon reservoir.

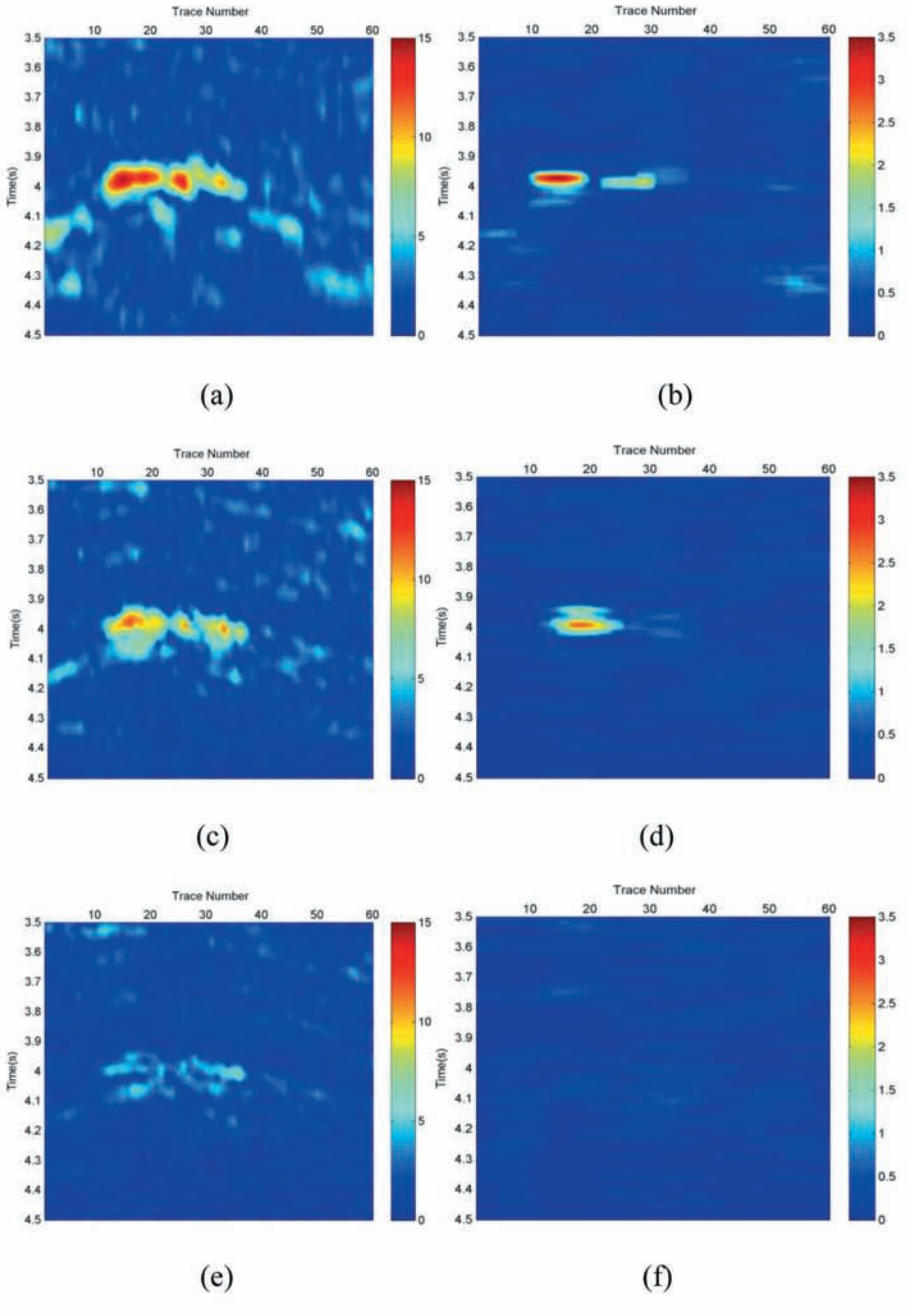

Fig. 5. (a), (c) and (e) are the frequency slices of 20 Hz, 30 Hz, and 40 Hz, using the CWT method. (b), (d) and (f) are the frequency slices of 20 Hz, 30 Hz, and 40 Hz, using the SDSC method. The variations in amplitude between frequency slices from SDSC-based results are clearer, and the energy is reduced rapidly.

Finally, we perform the CWT and SDSC on a 3D seismic data volume (Fig. 6) and extract the spectral time slices around 2250 ms. Fig. 7 displays the original amplitude map from the picked horizon. In this data set there are some faults between inlines 100 and 200 and crosslines 600 and 1000.

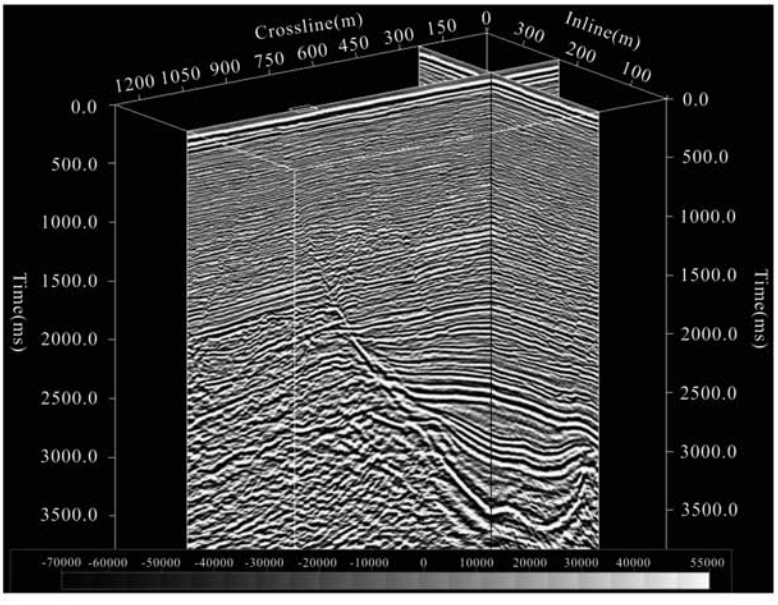

Fig. 6. A field data.

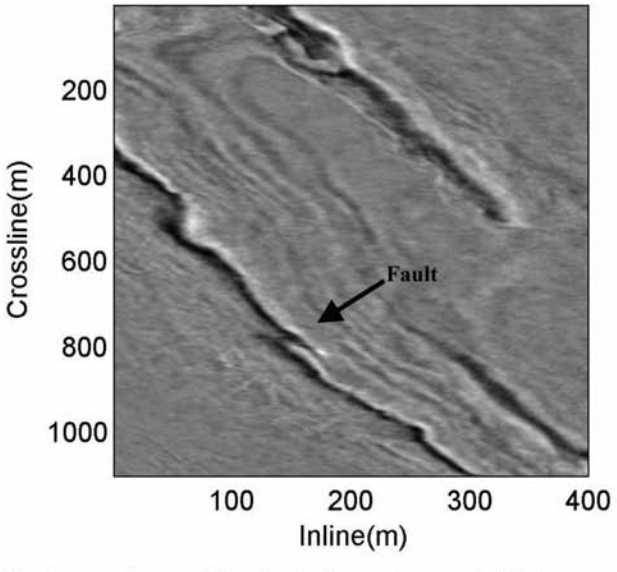

Fig. 7. Amplitude map from a 3D seismic data volume, which shows a fault feature.

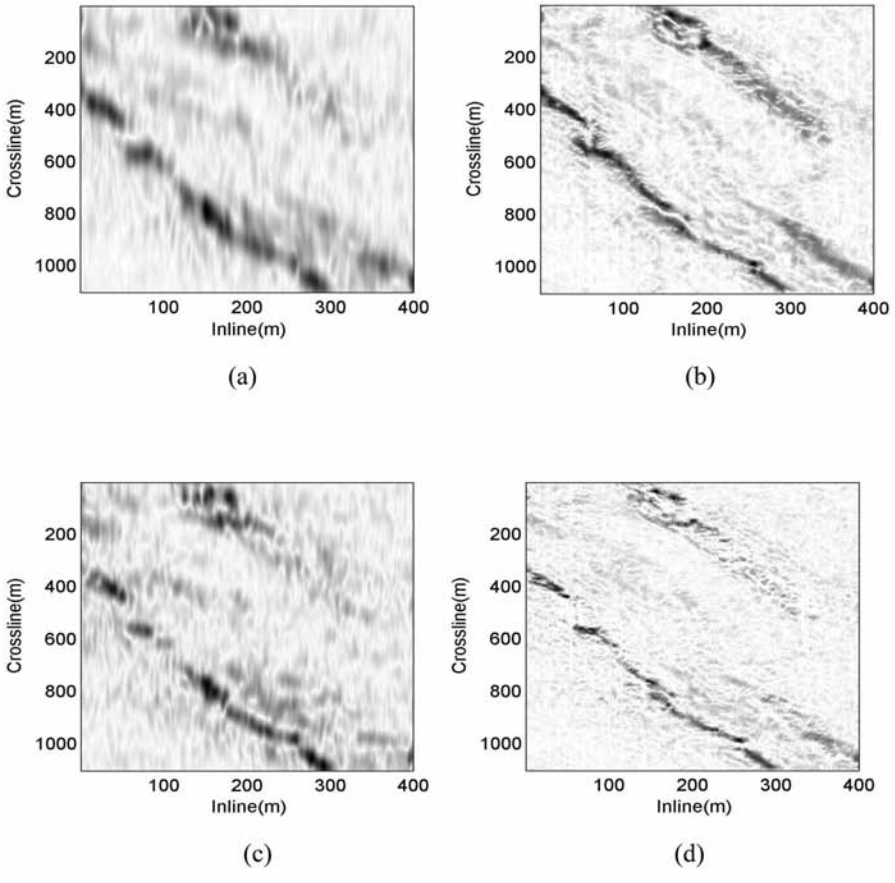

Fig. 8. (a) and (c) are 10 Hz and 25 Hz time slices obtained by using the CWT method. (b) and (d) are 10 Hz and 25 Hz time slices obtained by using the SDSC method. The SDSC-based spectral time slice shows a much clearer fault.

Figs. 8(a) and 8(c) show the spectral time slices of 10 Hz and 25 Hz for CWT. The results from SDSC-based method are displayed in Figs. 8(b) and 8(d), corresponding to 10 Hz and 25 Hz, respectively. It can be observed that both methods present some similar characteristics at the spectral time slices; however, there are still obvious differences among them, especially in the amplitude and spatial distribution of the fault. The CWT gives the blurred spectral time slices [Figs. 8(a) and 8(c)], which makes the further interpretation about the fault difficult. Compared with the CWT method, the SDSC-based spectral time slice shows much clearer fault [Figs. 8(b) and 8(d)], the variations in amplitude between different slices are very obvious, which contributes to estimating the trend and extent of the fault more effectively.

CONCLUSIONS

Spectral Decomposition with Sparsity Constraint (SDSC) obtains higher time-frequency resolution. Compared with the traditional spectral decomposition technique, CWT, the SDSC method shows a sparser time-frequency representation and is less sensitive to noise, which is beneficial to tracking the time-frequency energy locating the main seismic events in the trace effectively. Examples on two field sets show that the SDSC approach is more sensitive to hydrocarbon and more effective in detecting the low frequency anomaly associated with gas-charged reservoir. On the other hand, the spectral time slices are also present SDSC's potential in delineation of the subsurface structure and stratigraphic features, such as the fault, which is closely related with the oil and gas traps.

ACKNOWLEDGMENTS

We would like to thank the anonymous reviewer for constructive suggestions that greatly improved the manuscript. This work is supported by the National Key R&D Program of China (Grant No. 2016YFC0600102).

REFERENCES

Allen, J. B., 1977, Short term spectral analysis, synthetic and modification by discrete fourier transform. IEEE Transactions on Acoustics, Speech, and Signal Processing, 25, 235-238.

Beck, A. and Teboulle, M., 2009, A fast iterative shrinkage-thresholding algorithm for linear inverse problems. Siam J. Imaging Sci., 2: 183-202.

Bonar, D. and Sacchi, M., 2010, Complex spectral decomposition via inversion strategies. 80th Annual International Meeting, SEG, Expanded Abstracts: 1408–1412.

Bonar, D. and Sacchi, M., 2013, Spectral decomposition with f-x-y preconditioning. Geophys. Prospect., 61(suppl.1):152-165.

Castagna, J. P., Sun, S. and Siegfried, R. W., 2003, Instantaneous spectral analysis: detection of low-frequency shadows associated with hydrocarbons. The Leading Edge, 22: 120–127.

Chen, S., Li, X. and Wu, X., 2014, Application of frequency-dependent AVO inversion to hydrocarbon detection. J. Seismic Explor., 23: 241-264.

Chen, Y., Liu, T., Chen, X., Li, J. and Wang, E., 2014. Time-frequency analysis of seismic data using synchrosqueezing wavelet transform. J. Seismic Explor., 23: 303-312.

Cohen, L., 1966, Generalized phase-space distribution functions. J. Math. Phys., 7: 781-786.

Daubechies, I., Defrise, M. and Mol, C. D., 2004, An iterative thresholding algorithm for linear inverse problems with a sparsity constraint. Commun. Pur. Appl. Math., 57: 1413-1541.

Donoho, D., 2006, For most large underdetermined systems of linear equations, the minimalell-1 norm solution is also the sparsest solution. Commun. Pur. Appl. Math., 59: 907-934.

Farfour, M., Wang, J., Jo, Y. and Wan, K., 2013, Spectral decomposition and reservoir engineering data in mapping thin bed reservoir, Stratton field, South Texas. J. Seismic Explor., 22: 77-91.

Jeffrey, C. and William, J., 1996, On the existence of discrete Wigner distributions. IEEE Signal Proc. Let., 6:304-306.

Landweber, L., 1951, An iteration formula for Fredholm integral equations of the first kind. American Journal of Mathematics, 73: 615-624.

Liu, J. and Marfurt, K., 2007, Instantaneous spectral attributes to detect channels. Geophysics, 72: P23-P31.

Liu, W., Cao, S., Liu, Y. and Chen, Y., 2016. Synchrosqueezing transform and its applications in seismic data analysis. J. Seismic Explor., 25: 27-44.

Liu, Y. and Fomel, S., 2013, Seismic data analysis using local time-frequency decomposition. Geophys. Prospect., 61:516-525.

Mallat, S. and Zhang, Z., 1993, Matching pursuits with time frequency dictionaries. IEEE T. Signal Proces., 41: 3397-3415.

Marfurt, K. and Kirlin, R. L., 2001, Narrow-band spectral analysis and thin-bed tuning. Geophysics, 66: 1274–1283.

Odebeatu, E., Zhang, J. and Chapman, M., 2006, Application of spectral decomposition to detection of dispersion anomalies associated with gas saturation. The Leading Edge, 25: 206–210.

Partyka, G., Gridley, J. and Lopez, J., 1999, Interpretational application of spectral decomposition in reservoir characterization. The Leading Edge, 22: 353–360.

Portniaguine, O. and Castagna, J., 2004, Inverse spectral decomposition. 74th Annual International Meeting, SEG, Expanded Abstracts: 1786-1789.

Radad, M., Gholami, A. and Siahkoohi, H., 2016, A fast method for generating high resolution single-frequency seismic attributes. J. Seismic Explor., 25: 11-25.

Reine, C., M. van der Baan and R. Clark., 2009, The robustness of seismic attenuation measurements using fixed- and variable-window time-frequency transforms. Geophysics, 74: WA23-WA135.

Rioul, O. and Vetterlil. M., 1991, Wavelet and signal processing. IEEE Signal Proc. Mag., 8: 14-37.

Robinson, E.A. and Treitel, S., 1980, Geophysical Signal Analysis. Prentice-Hall, Inc.

Selesnick, I. \Sparse Signal Restoration." Connexions (2009) <http://cnx.org/content/m32168/1.3/>.

Sinha, S., Routh, P., Anno, P. and Castagna, J., 2005, Spectral decomposition of seismic data with continuous-wavelet transform. Geophysics, 70: 19–25.

Stockwell, R., Mansinha, L. and Lowe. R., 1996, Localization of the complex spectrum: the S transform. IEEE Trans. Signal Process., 44: 998–1001.

Wu, X., Chapman, M., Wilson, A. and Li, X., Estimating seismic dispersion from prestack data suing frequency-dependent AVO analysis. J. Seismic Explor., 23: 425-429.

Wu, X. and Liu, T., 2010. Analysis of seismic spectral attenuation based on Wigner-Wille distribution for sandstone reservoir characterization- a case study from West Sichuan Depression, China. J. Seismic Explor., 19: 69-85.

GUIDE FOR AUTHORS

Authors are invited to submit manuscripts of no more than 20 pp. to:
Journal of Seismic Exploration, Editorial Office, Urb. Los Flamingos, 29679 Benahavis, Spain. As PDF file or MS Word file to: jse@geophysical-press.com

Language
The journal will only contain articles in the English language.

Preparation of the text
a) The manuscript should be typewritten with double spacing and wide margins and include at the beginning of the paper an abstract of not more than 500 words. Words to be printed in italics should be underlined. The metric system should be used throughout.
b) The title page should include: the title, the name(s) of the author(s), and their affiliations.

References
a) References in the text with the name of the author(s) without initial(s), followed by the publication date in brackets.
b) If reference is made in the text to publications written by more than two authors, the name of the first author should be used, followed by "et al.". This indication, however, should never be used in the list of references. Here the names of all authors and co-authors should be mentioned.
c) The reference list should be in alphabetical order and on sheets separate from the text.

Tables
Tables should be compiled as separate sheets. A title should be provided for each table and they should be referred to in the text.

Illustrations
a) All illustrations should be numbered consecutively and referred to in the text.
b) Drawings should be completely lettered, the size of the lettering being appropriate to that of the drawings, but taking into account the possible need for reduction in size (of not more than 50%). The page format of the journal should be considered in designing the drawings.
c) Photographs must be of good quality, printed on glossy paper.
d) Figure captions should appear on the same page as the corresponding illustrations.

Proofs
One set of proofs will be sent to the author, to be checked for printer's errors.

Reprints
50 reprints of each article are supplied free of charge. Additional reprints can be ordered together with the return of the proofs.

Submission of manuscripts
Papers should be submitted to the Editorial Office of this journal, as a PDF or MS Word file. Submission of an article is understood to imply that the article is original and unpublished and is not being considered for publication elsewhere.

THERE IS NO PAGE CHARGE

JOURNAL OF

SEISMIC EXPLORATION

Volume 27, Number 1 **February 2018**

CONTENTS